

## Concentration dependent microstructure and transport properties of the magnetic semiconductor Gd-Si

E. Helgren, D. Queen, and F. Hellman

*Department of Physics, University of California Berkeley, Berkeley, California 94720*

L. Zeng

*Material Science Program, University of California San Diego, La Jolla, California 92093*

R. Islam and David J. Smith

*Center for Solid State Science and Department of Physics and Astronomy, Arizona State University, Tempe, Arizona 85287*

(Received 28 February 2007; accepted 6 March 2007; published online 11 May 2007)

The transport properties and microstructure of amorphous  $\text{Gd}_x\text{Si}_{1-x}$  alloys are presented. The conductivity increases from  $x=0$  through the metal-insulator transition ( $x=14$  at. %), up to a dopant concentration of 25 at. %. A sharp cusp in the magnitude of the conductivity is then observed and the flattening of the conductivity versus temperature curve occurs at higher concentrations. These transport results are explained in terms of high-resolution electron micrographs which demonstrate the formation of nano-crystallites at  $x \geq 25$  at. %. The flattening of the conductivity versus the temperature curve is identical to the results for annealing of  $a\text{-Gd}_x\text{Si}_{1-x}$  alloys with a low Gd concentration. © 2007 American Institute of Physics. [DOI: [10.1063/1.2727446](https://doi.org/10.1063/1.2727446)]

Magnetic dopants in semiconductors and alloys have experienced a resurgence of fundamental scientific research and technological interest in recent years. Metallic magnetic dopants provide a means to engineer both the electrical and magnetic properties of semiconductor systems. The widely studied III-V magnetic semiconductors GaMnAs and GaMnP are examples. Mn is a dopant for these systems, providing a means to tune the electrical properties while the  $d$ -shell electrons provide local moments which produce ferromagnetism via a hole-mediated exchange with Curie temperatures,  $T_C$ , up to 180 K.<sup>1,2</sup> Both the electrical and magnetic properties rely on the dopant concentration. Microstructural changes which occur at higher dopant concentration play an important role in the physical properties of doped semiconductors. For instance,  $T_C$  increases with increasing Mn concentration up to a critical concentration beyond which the clustering, dimer formation, and interstitial atomic location (as opposed to substitutional) limit further increases.

The rare earth element gadolinium is a common dopant in many applications because it is both a metal and an elemental ferromagnet, with a large net moment due to its half full  $f$  shell. Examples of technologically driven research on systems utilizing Gd include the magnetocaloric effect in Gd-Ge-Si alloys,<sup>3</sup> and the enhancement of photoluminescence in metal-oxide semiconductor light-emitting diodes upon incorporation of Gd, often through ion implantation.<sup>4,5</sup>

Our previous work has focused on the amorphous magnetic semiconductor  $a\text{-Gd}_x\text{Si}_{1-x}$  at concentrations close to the critical concentration  $x_C=14$  at. % (a typical value of  $x_C$  in metal semiconductor alloys) for the metal insulator transition (MIT).<sup>6,7</sup> An interesting physical behavior has been observed in the low temperature transport and magnetic properties of  $a\text{-Gd}_x\text{Si}_{1-x}$ , including the enormous negative magnetoresistance (MR).<sup>6,8,9</sup> The characteristic onset temperature,  $T^*$ , be-

low which the extremely large MR turns on, can be tuned by varying the Gd dopant concentration although  $T^*$  still remains below room temperature.<sup>8</sup>

Understanding the correlation between electrical properties and the microstructure of  $a\text{-Gd}_x\text{Si}_{1-x}$  as the dopant concentration is increased is not only relevant to possibly raising  $T^*$  for the observed large MR in  $a\text{-Gd}_x\text{Si}_{1-x}$  but may also provide insight for ion-implanted samples (it is well known that implantation leads to crystal damage resulting in an amorphous matrix<sup>10</sup>) and the III-V Mn-doped semiconductors. Previous studies for  $a\text{-Gd}_x\text{Si}_{1-x}$  alloys show a nonmonotonic trend in transport behavior with increasing Gd concentration.<sup>11</sup> We present here a systematic study of the microstructure and transport behavior over a wide range of  $x$  for  $a\text{-Gd}_x\text{Si}_{1-x}$ . With increasing Gd concentration, a correlation is found between the observation of nanocrystalline precursors (formation of small, identifiable equilibrium phase crystallites) in high-resolution electron micrographs, and an anomalous decrease in the magnitude of the conductivity  $\sigma(T)$  and the temperature coefficient of resistance (TCR)  $\alpha = (\rho(300\text{ K}) - \rho(4.2\text{ K})) / (\rho(4.2\text{ K})\Delta T)$  ( $\rho = 1/\sigma(T)$ ). Our transport results for  $a\text{-Gd}_x\text{Si}_{1-x}$  alloys are qualitatively similar to results for  $a\text{-Gd}_x\text{Si}_{1-x}$  alloys (for  $x=18, 27, 34, 37$ , and 46 at. %),<sup>11</sup> and to annealing results for lightly doped  $a\text{-Gd}_x\text{Si}_{1-x}$ ,<sup>12</sup> and can be explained in terms of the microstructural changes.

Amorphous  $a\text{-Gd}_x\text{Si}_{1-x}$  samples across a broad range of dopant concentrations from  $x=0$  to 50 at. % were prepared by electron-beam co-evaporation at a base pressure of  $10^{-9}$  Torr. Samples for transport measurements and electron microscope observations were grown on silicon-nitride coated Si substrates held at or below 70 °C. Film thicknesses determined by profilometry ranged from 1000 to 4000 Å. Thicknesses were also verified using Rutherford backscattering (RBS) on films co-deposited onto MgO sub-

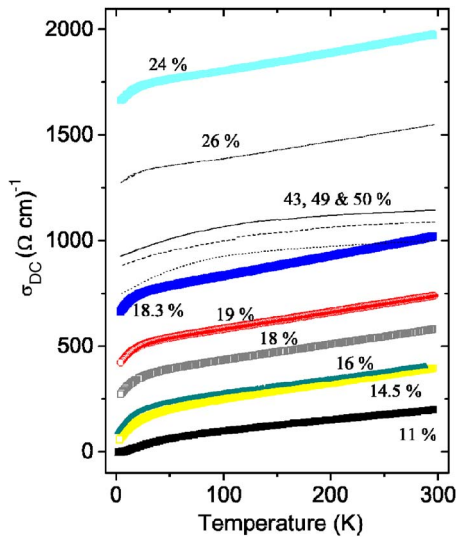


FIG. 1. (Color online)  $\sigma(T)$  for a wide range of  $a\text{-Gd}_x\text{Si}_{1-x}$  samples. Symbols show data for  $x$  from 11 to 25 at. % increasing monotonically. Dash-dot, solid, dashed, and dotted lines are  $x=26, 49, 43,$  and  $50$  at. %  $\sigma(T)$  data.  $\sigma(T)$  drops and becomes less temperature-dependent above  $x=25$  at. %, coincident with the formations of nanocrystalline precursors.

strates. RBS also provided the film stoichiometry to an accuracy of  $\pm 0.5$  at. %. Further details of sample preparation and characterization can be found elsewhere.<sup>8</sup> Standard four-probe measurement techniques were used to determine the dc conductivity data from a room temperature to 2 K.

The temperature-dependent dc conductivity,  $\sigma(T)$ , for a wide range of  $a\text{-Gd}_x\text{Si}_{1-x}$  doping concentrations is shown in Fig. 1. The symbols show samples for  $x < 25\%$ . These results show the general trend of monotonically increasing conductivity with increasing  $x$ . The lines are typical for  $25 < x < 50\%$  and show a slight decreasing trend with increasing  $x$ .

For samples close to but on the metallic side of the MIT, i.e., samples with  $x > x_C = 14$  at. %,  $\sigma(T)$  is well described by the relation  $\sigma(T) = \sigma_0 + A\sqrt{T} + BT$  which takes electronic correlations and weak localization effects into account for three-dimensional disordered electronic systems.<sup>6,13,14</sup> The transport data of the metallic samples fits this functional form quite well, with the prefactors  $A$  and  $B$  changing very little for  $x$  up to  $x=0.25$ . For  $x > 0.25$ ,  $\sigma(T)$  decreases and the curves change their relative shape, becoming less temperature-dependent. For samples on the insulating side of the MIT, the low temperature  $\sigma(T)$  displays the variable range hopping, a form of conduction with an exponential  $T$  dependence visible as a rounding of the low temperature data for the 11% sample in Fig. 1.

This concentration-dependent trend is captured in Fig. 2(a), which shows  $\sigma(4.2\text{ K})$  as a function of Gd concentration,  $x$ , for  $a\text{-Gd}_x\text{Si}_{1-x}$ . There is an increase in  $\sigma(4.2\text{ K})$  up to  $x=25$  at. % Gd with a sharp maxima, then a decrease up to 50 at. %. The concentration dependence of the TCR is plotted in Fig. 2(b). The TCR, in units of  $\text{K}^{-1}$ , defined as  $\alpha = (\rho(300\text{ K}) - \rho(4.2\text{ K})) / (\rho(4.2\text{ K})\Delta T)$ , with  $\Delta T = (300 - 4.2\text{ K})$  drops rapidly with increasing  $x$  through the MIT and up to 25%. This behavior is clearly a result of the very parallel nature of the transport curves below 25% giving an almost constant  $\Delta\sigma = \sigma(300\text{ K}) - \sigma(4.2\text{ K}) \cong 300(\Omega\text{ cm})^{-1}$

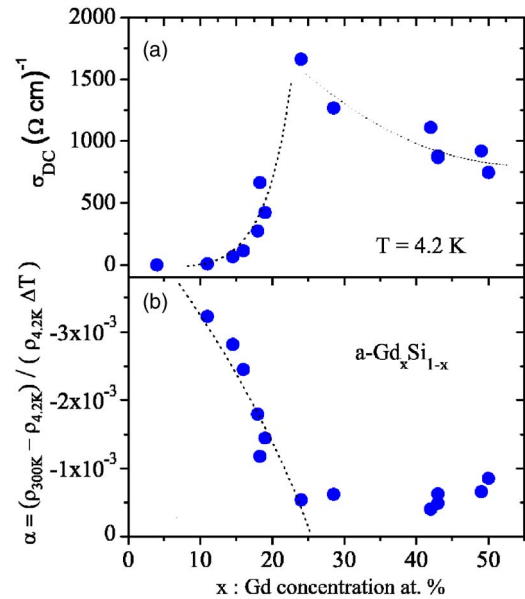


FIG. 2. (Color online) (a)  $\sigma(T=4.2\text{ K})$  for  $a\text{-Gd}_x\text{Si}_{1-x}$  alloys as a function of doping concentration. A maxima is visible at 25 at. %. (b) TCR,  $\alpha = (\rho(300\text{ K}) - \rho(4.2\text{ K})) / (\rho(4.2\text{ K})\Delta T)$ , vs Gd doping concentration.

such that the variation in  $\alpha$  is completely contained in the concentration dependence of  $\sigma_0 \sim \sigma(4.2\text{ K})$ .  $\alpha$  is constant and is approximately  $-0.5 \times 10^{-3}\text{ K}^{-1}$  for concentrations greater than  $x=25$  at. %.

Figure 3 shows high-resolution electron micrographs for  $a\text{-Gd}_x\text{Si}_{1-x}$  ranging from  $x=4$  to 41 at. %. For  $x=4$  and 14 at. %, the material is amorphous and homogeneous. EXAFS performed on samples in this low dopant concentration range have also shown that the Gd is not clustering. Thus, the individual Gd atoms can be considered as isolated, magnetic islands.<sup>15</sup> The electron micrographs for  $x=26$  and 41 at. % show small regions with lattice fringes corresponding to the formation of nanocrystallites. The predominant lattice fringe spacing on the micrographs is  $2.63\text{ \AA}$ , and some instances of fringe spacings of  $2.00$  and  $3.31\text{ \AA}$  are also present. Each of these spacings corresponds closely with lattice plane separations associated with crystalline hexagonal  $\text{GdSi}_2$ . Similar trends in microstructure from amorphous to

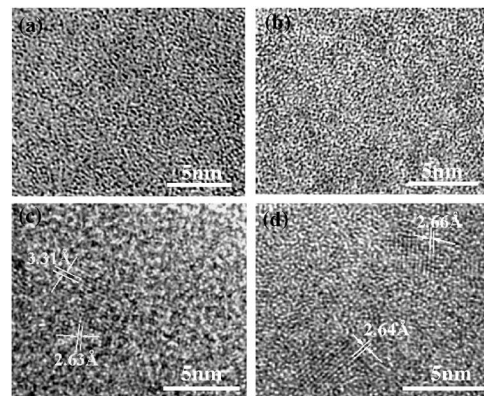


FIG. 3. High-resolution electron micrographs of  $\text{Gd}_x\text{Si}_{1-x}$  alloys. Panels (a)–(d) show samples with  $x=4, 14, 26,$  and  $41$  at. %. Panels (c) and (d) show lattice fringes indicating nanocrystalline regions with lattice spacing as labeled.

nanocrystalline have been reported for  $a\text{-Mo}_x\text{Ge}_{1-x}$  as probed by x-ray absorption fine structure, where distinct structural changes are found at  $x > 23$  at. %.<sup>16</sup>

Thus, the changes in the transport properties coincide with the onset of formation of nanocrystalline regions of  $\text{GdSi}_2$ . Hence a more complicated combination of percolation theory incorporating a Si-rich amorphous  $\text{Gd}_x\text{Si}_{1-x}$  matrix and small anti-ferromagnetic, metallic islands of  $\text{GdSi}_2$  (nominally  $\rho \approx 100 \mu\Omega \text{ cm}$ )<sup>17</sup> which may also affect magnetic scattering, must be utilized for dopant concentrations above 25 at. %.

The trends visible in the transport behavior are similar to previous results for annealing  $a\text{-Gd}_x\text{Si}_{1-x}$ .<sup>12</sup> For a fixed  $x$ -value, vacuum annealing caused formation of nanocrystalline  $\text{GdSi}$  and  $\text{GdSi}_2$  precipitates, with increasing volume fraction of these nanocrystalline regions with increasing annealing temperature. The overall effect on the transport with annealing was the cause of the  $\sigma(T)$  curves to flatten, identical to the changes seen in the  $\sigma(T)$  curves upon increasing the dopant concentration to greater than 25 at. % and for identical reasons.

In summary, we have reported the transport properties and microstructural properties of  $a\text{-Gd}_x\text{Si}_{1-x}$ . The experimental evidence supports the conclusion that the electrical transport is altered because nano-crystalline regions of  $\text{GdSi}_2$  start to form in an otherwise homogeneous system at doping levels greater than 25 at. %. The trend in the high concentration transport results are qualitatively identical to published reports on the doping dependence of  $\sigma(T)$  in  $\text{Gd-Ge}$ .<sup>11</sup> The microstructural evidence provides a clear indication of what

type of transport theory is appropriate depending on the dopant concentration.

We acknowledge use of the facilities in the John M. Cowley Center for High Resolution Electron Microscopy at Arizona State University, and we thank Barry Wilkens for assistance with RBS. This research was supported by the NSF DMR.

- <sup>1</sup>I. Zutic, J. Fabian, and S. Das Sarma, *Rev. Mod. Phys.* **76**, 32 (2004).
- <sup>2</sup>P. Kacman and I. Kuryliszyn-Kudelska, *Local-Moment Ferromagnets* (Springer, New York, 2005).
- <sup>3</sup>V. K. Pecharsky and K. A. Geschneidner, *Phys. Rev. Lett.* **78**, 4494 (1997).
- <sup>4</sup>J. M. Sun, S. Pruncal, W. Skorupa, M. Helm, L. Rebohle, and T. Gebel, *Appl. Phys. Lett.* **89**, 091908 (2006).
- <sup>5</sup>J. M. Sun, W. Skorupa, T. Dekorsy, M. Helm, L. Rebohle, and T. Gebel, *Appl. Phys. Lett.* **85**, 3387 (2004).
- <sup>6</sup>F. Hellman, M. Q. Tran, A. E. Gebala, E. M. Wilcox, and R. C. Dynes, *Phys. Rev. Lett.* **77**, 4652 (1996).
- <sup>7</sup>G. Hertel, D. J. Bishop, E. G. Spencer, J. M. Rowell, and R. C. Dynes, *Phys. Rev. Lett.* **50**, 743 (1982).
- <sup>8</sup>E. Helgren, J. J. Cherry, L. Zeng, and F. Hellman, *Phys. Rev. B* **71**, 113203 (2005).
- <sup>9</sup>E. Helgren, L. Zeng, K. Burch, D. Basov, and F. Hellman, *Phys. Rev. B* **73**, 155201 (2006).
- <sup>10</sup>M. J. Madou, *Fundamentals of Microfabrication* (CRC, New York, 2002).
- <sup>11</sup>R. J. Gambino and T. R. McGuire, *IEEE Trans. Magn.* **19**, 1952 (1983).
- <sup>12</sup>E. Guillotel, L. Zeng, E. Helgren, F. Hellman, R. Islam, and D. J. Smith, *J. Appl. Phys.* **101**, 023908 (2007).
- <sup>13</sup>P. A. Lee and T. V. Ramakrishnan, *Rev. Mod. Phys.* **57**, 287 (1985).
- <sup>14</sup>N. Mott, *Metal-Insulator Transitions* (Taylor and Francis, London, 1990).
- <sup>15</sup>D. Haskel, J. W. Freeland, J. Cross, R. Winarski, M. Neville, and F. Hellman, *Phys. Rev. B* **67**, 115207 (2003).
- <sup>16</sup>J. B. Kortright and A. Bienenstock, *Phys. Rev. B* **37**, 2979 (1988).
- <sup>17</sup>C. Boragno, M. R. Bonansinga, and F. Nava, *Solid State Commun.* **92**, 515 (1994).